Soft Matter

PAPER

View Article Online
View Journal | View Issue

Cite this: *Soft Matter*, 2025, **21**, 1699

Soft and tough cellulose nanocrystals interlocked with polyacrylate-bearing cyanobiphenyl ionogels through a double network strategy†

Patrick K. Njenga,[a] Francis K. Masese,[a] Dennis M. Ndaya,[b] M. Daniela Morales-Acosta,[b] Nicholas Eddy[b] and Rajeswari M. Kasi *[ab]

There are several examples of double network gels prepared from cellulose nanocrystals (CNC) conjugated with water-soluble polymers. However, soft but tough gels composed of mostly CNCs have been challenging to design due to aggregation or precipitation of CNCs at higher concentrations in solvated and gelled systems. We report a general strategy to introduce covalent and non-covalent interactions within cellulose nanocrystals (CNCs) to develop tough, processable, liquid crystalline (LC) gels. A liquid crystalline 12-methylene spacer cyanobiphenyl (CB12OH), is grafted onto acrylic acid *via* Steglich esterification and subsequently copolymerized with acrylic acid *via* free radical polymerization to afford an amphiphilic liquid crystalline polymer (LCP), PAACB12-r-PAA. The free carboxyl (COOH) groups from polyacrylic acid (PAA) in the copolymer are randomly interlocked with the hydroxyl (OH) groups of CNC through covalent crosslinking and host–guest supramolecular hydrogen bonding in DMSO and 1-butyl-3-methylimidazolium acetate ionic liquid. The dominant cyanobiphenyl–cyanobiphenyl (CB12–CB12) interactions yield hierarchically structured, tough, free-standing liquid crystalline nanocomposite ionogels. Rheological studies of the interlocked free-standing ionogels display a typical crosslinked gel behavior with the storage moduli (G') ranging 10^3–10^4 Pa across the entire angular frequency range. Mechanical properties are tailored by varying the concentration of CNCs in the nanocomposite gel. This facile design provides a general strategy to prepare soft and tough liquid crystalline gels from renewable resources.

Received 26th November 2024,
Accepted 29th January 2025

DOI: 10.1039/d4sm01409j

rsc.li/soft-matter-journal

Introduction

Cellulose nanocrystals (CNCs) are rod-like, charged, semicrystalline materials with dimensions ranging from 5 to 20 nm in width and 100 to 500 nm in length and prepared through either the acidic or alkaline hydrolysis of cellulose biopolymers.[1–4] In lyotropic solutions, CNCs self-assemble into cholesteric or chiral nematic (Ch*) liquid crystalline (LC) mesophases.[5–7] Dried thermotropic films of CNCs show retention of the cholesteric mesophase with optical reflection controlled by the pitch of the cholesteric helix and the temperature of the system.[8–10]

There are several roadblocks to the use of CNCs as a sustainable and renewable LC material. CNCs have poor solubility in different solvents and lack a ''chemical'' handle within the structure to attain optimal viscoelastic, mechanical, and processing features in films and gels with retention of their LC properties.[8,11–15] To address some of these shortcomings, molecular liquid crystals (LCs) or liquid crystalline polymers (LCPs) are grafted onto CNCs to (i) manipulate self-assembly through a variety of LC–LC interactions, and produce nematic, chiral nematic with tunable pitch length, and non-nematic smectic mesophases[5,16–18] and (ii) enhance dispersion and solubility in different solvents including ionic liquids.[8,19] For example, Hegman and Chang showed that 4 or 5-methylene spacers are used to attach thermotropic LCs to CNCs to improve the solubility of CNCs in organic solvents.[20] Masese and coworkers demonstrated that when a cyanobiphenyl LC molecule with 12-methylene spacer (CB12) is appended onto a CNC backbone, CB12–CB12 LC interactions dominate over CNC–CNC LC interactions, tuning the isomorphism of CNC from the lyotropic chiral nematic LC phase to smectic LC phase with improved colloidal solubility in organic solvents such as DMSO.[8] Covalently linking CNC with LCPs is known to enhance the colloidal stability of resulting suspensions as shown by Risteen and coworkers[19] In another example, Muller and

[a] *Department of Chemistry, University of Connecticut, Storrs, CT 06269, USA. E-mail: rajeswari.kasi@uconn.edu; Tel: +1 860-486-4713*
[b] *Institute of Materials Science, University of Connecticut, CT 06269, USA*

† Electronic supplementary information (ESI) available. See DOI: https://doi.org/10.1039/d4sm01409j

coworkers prepared photoresponsive azo molecules attached to CNCs and these molecules are dispersed into a polyurethane acrylate matrix at different concentrations. Samples with 10, 15, and 20 wt% of azobenzene-bearing CNC displayed a shear thinning tendency whereas percolation of the nanocellulose network led to a first plateau region along with $G' > G''$ at low shear stress. However, a decrease in G' and an increase in G'' are reported at higher stress. This occurrence held till $G' = G''$, the dynamic yield stress region.[21] These examples show that the colloidal solubility of CNCs can be enhanced by covalently attaching a molecular LC or LCP. However, the preparation of tough, viscoelastic gels with quantitative retention of LC structure and good compressive strength from CNCs remains unexplored.

Different approaches to toughen hydrogels have gained tremendous research effort over the last decade. For instance, Gong and coworkers reported the classical double network strategy proposed by Gong comprised of two structurally contrasting interpenetrating networks (IPN): a highly crosslinked, low concentration, brittle, and strong polyelectrolyte as the first network and a lowly crosslinked, high concentration and ductile network polymerized onto the swollen polyelectrolyte.[22] There are several double networks (DN) from CNC with different conventional polymers[8,23–29] but the double network involving CNC with different liquid crystalline polymers (LCPs) where there is retention of LC properties (from both CNC and LCP) after interlocking remains unexplored.[8]

Employing the double network strategy, we report the synthesis of a new platform comprising a small thermotropic liquid crystal (CB12) grafted onto a flexible poly(acrylic acid) backbone and subsequently interlocked with CNC using 1-ethyl-3-(3-dimethylamino propyl) carbodiimide hydrochloride (EDC) crosslinker. The flexible PAACB12-r-PAA acts as the dangling chain thereby giving a high osmotic pressure that increases the swelling degree and enhances the rigidity of the first network. CNC is then introduced as the second interpenetrating network and crosslinked with the free COOH groups from the copolymer using EDC (Fig. 1). The presence of (i) host–guest interactions such as hydrogen bonding, van der Waals, and LC–LC interactions as well as (ii) chemical conjugation through covalent bonding yields tough CNC–LCP nanocomposite gels with retained LC structure. Adopting CNC as a filler material leads to a breakthrough in the design of sustainable hybrid gels with tailored toughness and morphology.

Experimental

Dual interlocking of LC-containing copolymer with CNC

Representative amounts of PAACB12-r-PAA and EDC (Table 1) are transferred to a clean, oven-dried 50 ml round-bottomed flask equipped with a magnetic stir bar. 0.25 ml DMSO and 0.75 ml 1-butyl-3-methylimidazolium acetate are added, and the flask is sealed using a rubber septum. The reaction mixture is purged with nitrogen for 5 min and stirred in an oil bath for 4 h at 60 °C. CNC (Table 1) is dissolved in 2 ml of 1-butyl-3-methylimidazolium acetate and 1 ml of DMSO then added dropwise to the reaction mixture followed by purging for 5 min using nitrogen. The mixture is allowed to react for 8 h, cooled to room temperature, and carefully transferred into a 20 mm mold to gel gradually. The interlocking pathway is shown in Fig. 1 below. [BMIM][AC] is chosen as the ionic liquid since the $[BMIM]^+$ cation dissolves CNC with the help of DMSO. In our hybrid LCP (CNC-i-PAACB12-r-PAA) ionogels, the negligibly volatile ionic liquid is retained in the interconnected 3D pore structure of the hybrid LCP.[30] [BMIM][AC] also acts as a hydrogen bond acceptor, enhancing host–guest interactions between CNC and COOH groups in the PAACB12-r-PAA copolymer yielding tough-soft ionogels.[30]

Results and discussion

Synthesis of dual network nanocomposite gels

Synthesis of the modified liquid crystalline random copolymer is adopted from a previous study.[31] In a clean oven-dried 250 ml flask, equipped with a magnetic stir bar, purified AACB12 (364 mg 839.5 mmol), acrylic acid, AA (94.5 mg 1310.8 mmol), and azobisisobutyronitrile, AIBN (2.4 mg 14.7 mmol) are charged and dissolved in 10 ml of anhydrous toluene. The mixture is then purged for 5 min using nitrogen gas and allowed to proceed at 70 °C and 300 rpm for 6 h.

The crude product is then precipitated in cold methanol and dried overnight in a vacuum oven set at 45 °C. This random copolymer is structurally a polyelectrolyte composed of a poly(acrylic acid) backbone covalently bonded to a liquid

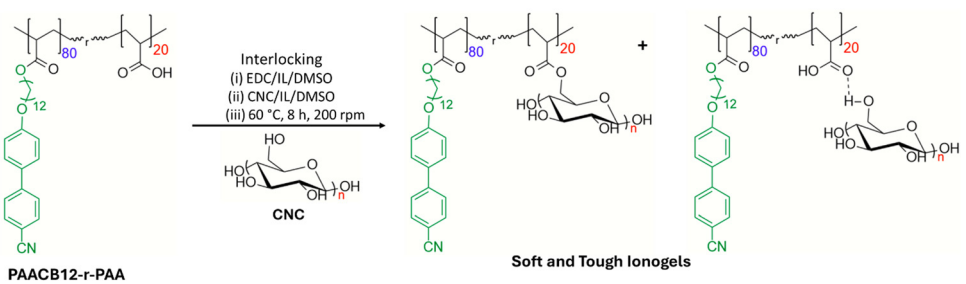

Fig. 1 Synthetic pathway showing dual network CNC-i-PAACB12-r-PAA nanocomposite ionogels using 40 wt% EDC in 1/3 v/v% 1-butyl-3-methylimidazolium acetate/DMSO.

Table 1 PAACB12-r-PAA copolymer and CNC feed ratios in nanocomposite ionogels using 40 wt% EDC as the crosslinker in 1/3 v/v% 1-butyl-3-methylimidazolium acetate/DMSO

Ionogels	PAACB12-r-PAA	CNC	IL	DMSO	EDC
100_0 wt%	100 mg	0 mg	0.75 ml	0.25 ml	40 mg
95_5 wt%	95 mg	5 mg	0.75 ml	0.25 ml	40 mg
80_20 wt%	80 mg	20 mg	0.75 ml	0.25 ml	40 mg
65_35 wt%	65 mg	35 mg	0.75 ml	0.25 ml	40 mg
50_50 wt%	50 mg	50 mg	0.75 ml	0.25 ml	40 mg

crystalline cyanobiphenyl unit and with free COOH units. These available COOH functional groups are used for interlocking and physical assembly with CNC enhancing the mechanical properties of the resultant nanocomposite ionogels. The synthetic pathway for CB12OH, AACB12 monomer, as well as PAACB12-r-PAA copolymer is shown in Fig. S1 (ESI†). Successful synthesis of these molecules was investigated using ^{1}H NMR (Fig. S2–S4, ESI† respectively). In the stacked ^{1}H NMR (Fig. S5, ESI†), geminal protons between 6.27 ppm and 5.59 ppm, as well as a vicinal proton at 6.05 ppm, indicate the presence of a double bond in the monomer. Cyanobiphenyl protons appear at 7.05 ppm, 7.68 ppm, and 7.84 ppm indicating complete attachment of the thermotropic LC. The ester connection peaks at 3.97 ppm while the proton adjacent to the ether is a contribution from the LC molecule. We further utilize free OH functional groups from CNCs to physically (H-bonding, LC–LC interaction, and supramolecular van der Waals forces) and chemically (covalent bonds) interlock the copolymer *via* dual crosslinking chemistry.[32,33] The interlocked system (CNC-i-PAACB12-r-PAA) is identified using FTIR studies as shown in Fig. S6 (ESI†). Bands at 2224.7 cm^{-1}, 1715.8 cm^{-1}, 3297.5 cm^{-1}, 1247.2 cm^{-1}, 2850.7 cm^{-1} and 2918.2 cm^{-1} correspond to the strong stretching bands of C≡N, C=O, O–H, C–O, and C–H respectively. The corresponding feed ratios for PAACB12-r-PAA and CNC are shown in Table 1 below.

Yield test

2 ml of the cooled reaction mixture is transferred to three 20 mm molds for rheological studies. From this, a 1 ml aliquot is transferred into a 10 ml scintillation vial and allowed to gel for 72 h for yield tests by monitoring flow. Phase map studies are performed by varying the feed ratios of PAACB12-r-PAA copolymer and CNC as shown in Table 1. CNC-i-PAACB12-r-PAA nanocomposite ionogels consisting of a porous solid whose pores are pervaded with 1-butyl-3-methylimidazolium acetate ionic liquid and DMSO are shown in Fig. 2.

Microstructural studies

To discern the microstructural changes resulting from side chain LC surface functionalization onto the PAA backbone as well as the incorporation of CNC into the copolymer network, we conduct the wide-angle X-ray scattering (WAXS) studies of the LC, LCP, and nanocomposite ionogels (Fig. 3). CNC used is reported to exhibit four main diffraction peaks at 2θ = 14.6°, 16.4°, 20.3° and 22.5° with a crystallinity index of 87% and a crystallite size of about 6.3 nm. These microstructural features resemble those exhibited by Cellulose I_β crystalline structure (Monoclinic unit cell, ICDD PDF 00-056-1718).[2] The side chain CB12 LC displays distinct diffraction peaks at 2θ = 5.6°, 17.5°, 20.9°, 22.4°, 24.8°, 25.4° and 28.7° which corresponds to LC packing *d*-spacing of 15.9 Å, 5.1 Å, 4.1 Å, 4.3 Å, 3.7 Å, 3.5 Å and 3.1 Å respectively. Upon chemical interlocking to afford CNC-i-PAACB12-r-PAA, the WAXS diffraction pattern changes significantly. PAACB12-r-PAA displays a strong diffraction peak at 2θ = 22.4° as well as broad diffraction peaks at 2θ = 25.7°and 28.7° (corresponding to 4.0 Å, 3.6 Å, and 3.1 Å) which represent π–π* stacking from the cyanobiphenyl LC in the copolymer backbone. The sharp diffraction peak for PAACB12-r-PAA (2θ = 22.4°) compared to that of the nanocomposite ionogels suggests that the introduction of CNC as a plasticizer to the system increases the pliancy of the polymer chain thus modifies the microstructure of the resultant nanocomposite ionogels.[34,35] 80_20 wt% ionogels have diffraction peaks at 2θ = 17.9°, 20.5°, 22.4° and 24.8° with corresponding *d*-spacings of 5.0 Å, 4.4 Å, 4.1 Å, and 3.7 Å respectively traceable to CB12 LC packing. These two diffraction patterns from the CB12 and LCP suggest that the enchainment of PAA into the system does not mask the liquid crystallinity of CB12 entirely but reduces the intensity and shifts the peak position due to the flexibility of the chains.

Based on our prior work on cellulose-CB12 and PAA-CB12 systems, we expect that CB12–CB12 interactions result in polymorphic interdigitated smectic mesophase[8,31,36] as shown by

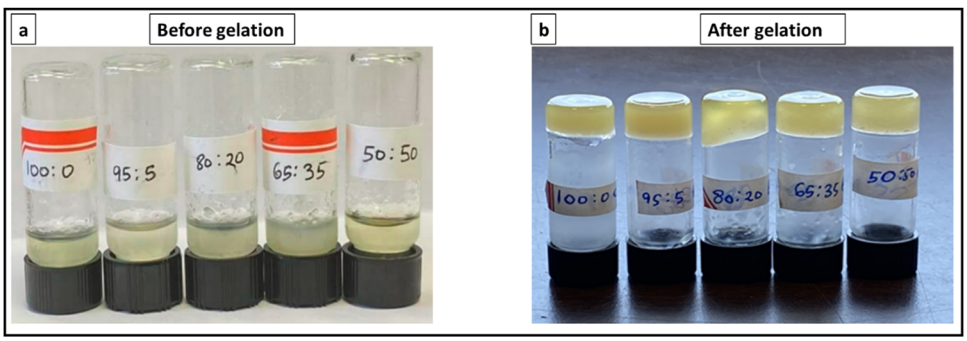

Fig. 2 Yield results for CNC-i-PAACB12-r-PAA gels at room temperature. (a) before gelation (b) after 24 h gelation in 1-butyl-3-methylimidazolium acetate ionic liquid/DMSO using EDC.

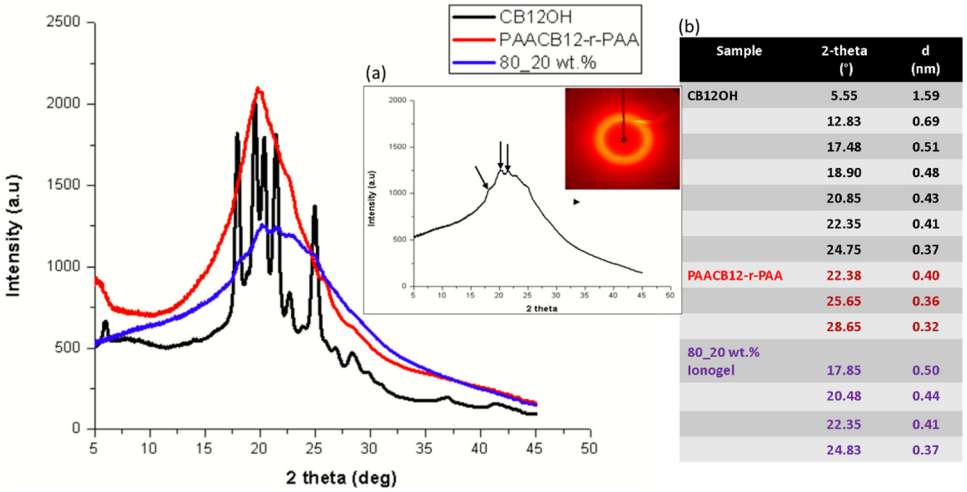

Sample	2-theta (°)	d (nm)
CB12OH	5.55	1.59
	12.83	0.69
	17.48	0.51
	18.90	0.48
	20.85	0.43
	22.35	0.41
	24.75	0.37
PAACB12-r-PAA	22.38	0.40
	25.65	0.36
	28.65	0.32
80_20 wt.% Ionogel	17.85	0.50
	20.48	0.44
	22.35	0.41
	24.83	0.37

Fig. 3 Wide angle X-ray scattering (WAXS) results for CB12OH, PAACB12-r-PAA, and interlocked ionogels. Inserts: (a) 1D and 2D WAXS results for 80_20 wt% interlocked ionogels (b) table showing calculated *d*-spacings (nm).

the room temperature small angle X-ray scattering (SAXS) results, Fig. S16 (ESI†).

We perform UV reflectance measurements to probe further the mesophases formed by the liquid crystal polymers and the interlocked system. We prepared free-standing films (~0.5 mm thick) by hot pressing at 85 °C for 1 h. The sample was quenched to room temperature using cold air to induce self-assembly and mesophase formation. The broad reflection spectra of CNC showed a typical 1D cholesteric mesophase formation as shown in Fig. S13 (ESI†).[37] The liquid-crystalline PAACB12-r-PAA and the interlocked CNC-i-(PAACB12-r-PAA) nanocomposite show the presence of a smectic mesophase characterized by CB12 reflection in the deep UV region.[38] The large CB12 domains in PAACB12-r-PAA and CNC-i-(PAACB12-r-PAA) reduced the transparency of the film samples, thus increasing the scattering of incident light with maximum wavelength (λ_{max}) at 275 nm and 276.5 nm, respectively, which can be attributed to the π–π^* transmission bands.[39,40] These two transmission wavelengths appear blue-shifted relative to the neat CB12 moiety reported at ~300 nm.[38,39,41] These microstructural studies are confirmed by evaluating their surface morphology using polarized optical microscopy (POM). Images show a characteristic smectic surface PAACB12-r-PAA and CNC-i-(PAACB12-r-PAA), as shown in Fig. S12 (a)–(c) (ESI†).[42,43] CNC exhibited a surface, typical of a cholesteric mesogen, Fig. S12(d) (ESI†).[44,45]

Rheological properties

The effect of different concentrations of CNC on the viscoelastic properties of the ionogels is investigated through rheological measurements. First, amplitude sweeps as shown in Fig. 4 are carried out to determine the linear viscoelastic (LVE) region for the ionogels. We observe significant improvement in the storage modulus of the CNC-i-PAACB12-r-PAA ionogels with the addition of CNC. The modulus generally increased with an increase in wt% of the CNC, enhancing the mechanical stability of these ionogels.[46–49] For example, the addition of 5 wt% of CNC led to a significant increase in the storage modulus of the nanocomposite ionogels ($\approx 10^4$ Pa) relative to the neat copolymer gels ($\approx 10^2$ Pa). The structure of nanocomposite ionogels remains unperturbed below 1% strain with $G' > G''$ while beyond 1% strain, the nanocomposite ionogels report a sharp decrease in the modulus. The subsequent rheological studies were conducted using 0.5% strain to keep the ionogels within the LVE region.

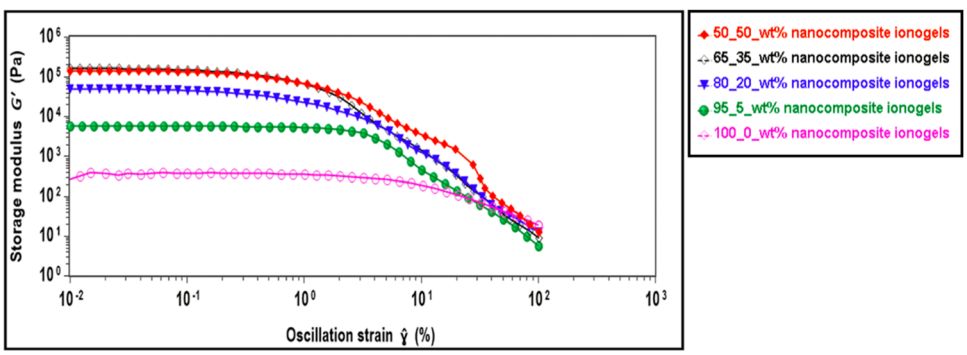

Fig. 4 Strain sweep results for CNC-i-PAACB12-r-PAA ionogels with varying CNC concentration.

Polymer nanocomposite gels and blends have been reported to undergo rearrangement in both macro and microstructure over time.[24,50–53] Structural changes resulting from these rearrangements influence their rheological behavior and can be examined through oscillatory time sweep experiments.[54–56] CNC-i-PAACB12-r-PAA ionogels are subjected to these oscillatory time sweep studies to determine their structural stability over time and the results for storage and loss moduli with time reported (Fig. 5). All nanocomposite ionogels remain structurally stable over the entire step time (1800 s).

Frequency sweep experiments are performed in the linear viscoelastic range (LVR) for the neat copolymer and the nanocomposite ionogels over the frequency of 0.01–100 Hz at a strain of 0.5% and a constant temperature of 25 °C. Fig. 6 compares the frequency dependence of the storage (G') and loss modulus (G'') of CNC-i-PAACB12-r-PAA gels prepared using 0, 5, 20, 35, and 50 wt% of CNC. For all the gels except at higher frequency, G' is frequency independent and G'' is one order of magnitude smaller than G'. The values for storage modulus (G') dominate the loss modulus (G'') ($G' > G''$) for all the gels and this confirms their inherent high mechanical properties, flexibility, and elastic properties.[57–60] The general trend across all gel concentrations indicates an increase in both G' and G'' with an increase in wt% CNC for all the samples. Optimum gel strength is reported for 50_50 wt% nanocomposite gel. This observed trend can be attributed to the dual crosslinking network resulting from the synergistic covalent attachment and host–guest interactions between the COOH of the LC-containing copolymer and free OH in CNC.[61–63] Neat copolymer ionogels (100_0 wt%) had the least storage and loss moduli relative to the rest of the nanocomposites.[62,64–66] This improved gel stability with increasing CNC concentration justifies the reported use of CNC as a good sustainable, and biodegradable filler material in this regime.[67–69]

Further understanding of the crosslinked ionogels' ability to dissipate mechanical energy or internal friction *via* segmental motion,[70] is seen in the tan delta with frequency plot. The tangent of the phase angle ($\tan\delta$) is plotted against frequency where the phase angle becomes smaller as the material becomes more elastic and increases as the material becomes less elastic material as described by the tan delta equation below.

$$\tan\ \delta = \frac{\text{Loss modulus}\ (G'')}{\text{Storage modulus}\ (G')}$$

A high tan delta shows less elastic material while a low tan delta shows more elastic material. 100_0 wt% ionogel has the highest tan delta value making it less elastic compared to the rest of the samples. 50_50 wt% on the other hand has the least tan delta making it the most elastic. We confirm that introducing CNC to our system increases the networking thereby improving the elasticity of the PAACB12-r-PAA. This sweep is conducted at a constant temperature of 25 °C as shown in Fig. 7.

We examine the viscous or unrecoverable regions of our copolymer and nanocomposite ionogels using complex viscosity with frequency sweep at constant temperature. Fig. 8 shows the dependency of complex viscosity in the copolymer and nanocomposite ionogels on angular frequency with varying CNC concentrations at 25 °C. A typical non-Newtonian

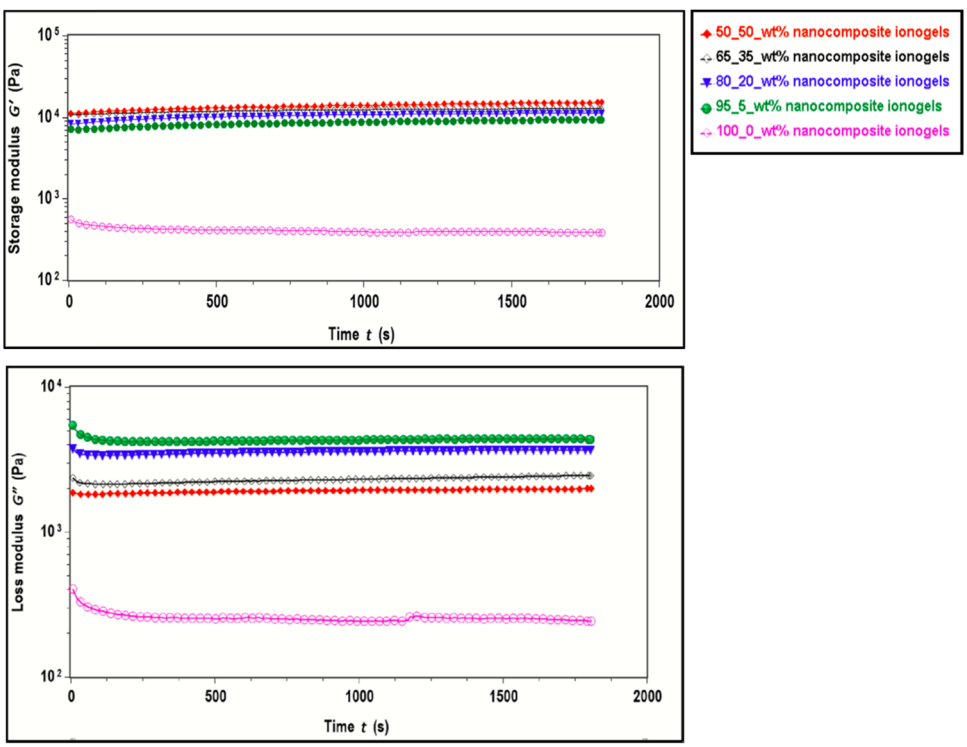

Fig. 5 Time sweep results showing structural stability of PAACB12-r-PAA copolymer and CNC-i-PAACB12-r-PAA ionogels over time at room temperature.

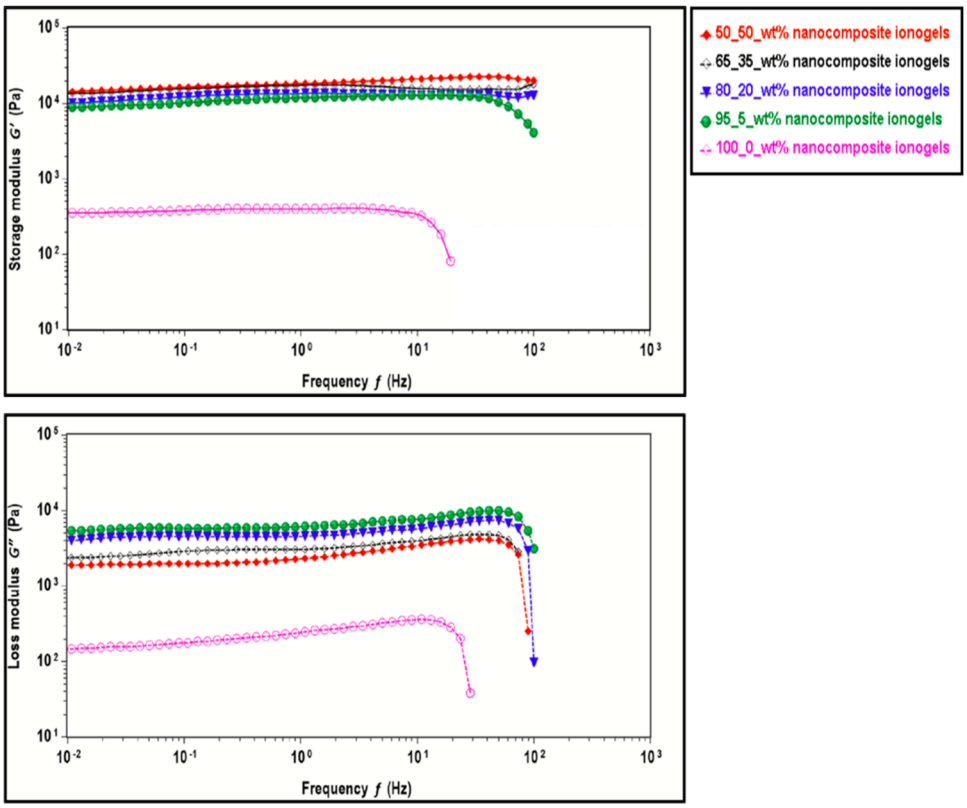

Fig. 6 Frequency dependence of the storage (G') and loss modulus (G'') of the neat copolymer and CNC-i-PAACB12-r-PAA ionogels prepared by 0, 5, 20, 35, and 50 wt% of CNC using 0.5% strain at 0.01–100 Hz frequency and a constant temperature of 25 °C.

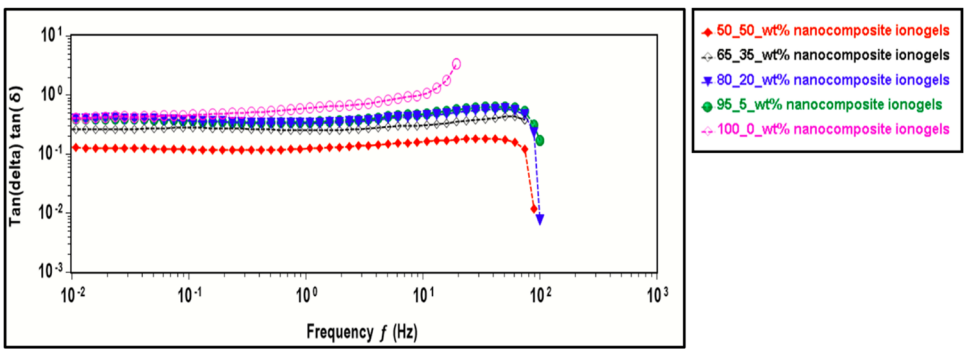

Fig. 7 Tan delta *vs.* angular frequency sweep for CNC-i-PAACB12-r-PAA nanocomposite ionogels at 25 °C.

(frequency-dependent) behavior is reported for all the sample concentrations where we observe a significant increase in the complex viscosity of the ionogels with increasing CNC concentrations. This is mostly due to the reduced volume fraction of the unbound free solvent in the ionogels resulting from increased CNC concentration. For a constant volume of DMSO/IL, each additional CNC increases the interactions thereby the network. 50_50 wt% ionogels, for instance, has a robust network thus reducing the unbound solvent layer further and reporting a complex viscosity of 2 orders of magnitude higher than 100_0 wt% which serves as the control. This reduction in complex viscosity with angular frequency shows that the reciprocal of the characteristic relaxation time ($1/\tau_\eta$) is smaller than the angular frequency (ω).

Tan delta *vs.* temperature ramp for 50_50 wt% CNC-i-PAACB12-r-PAA ionogel with 40 wt% EDC is conducted at 1Hz frequency with an oscillatory strain of 0.5% and a constant temperature of 25 °C as shown in Fig. S11 (ESI†). The tan delta dramatically drops from about 1.25 to 1.0 when the sample is heated from −70 °C to −59.6 °C then steadily drops to about 0.3 upon heating from −59.6 °C to −45 °C. Further temperature increase shows a gradual decrease in the tan delta to about 0.09 at 100 °C. In this region, a slow but steady reduction in the tan delta of the material gives it a quasi-continuous state where the tan delta

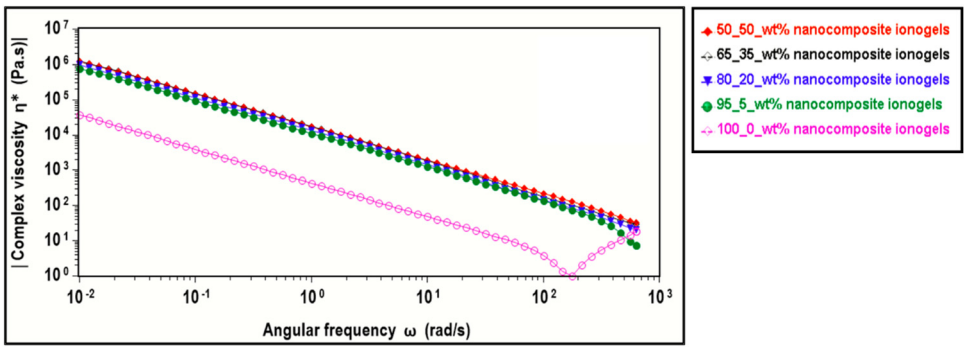

Fig. 8 Complex viscosity *vs.* angular frequency sweep showing the frequency-dependence of PAACB12-r-PAA copolymer and CNC-i-PAACB12-r-PAA ionogels with varying CNC concentrations at 25 °C.

decrease shows a plateau. Above 100 °C, the sample loses its elasticity, and the tan delta measurements become unreliable.

The integration of CNC filler in the polymer network during interlocking influences the mechanical robustness of the resultant nanocomposite ionogels. We monitor this influence by comparing the stress–strain curves for 100_0 wt% CNC-i-PAACB12-r-PAA (unfilled) and 50_50 wt% CNC-i-PAACB12-r-PAA as shown in Fig. 9 below. From the results, a 50 wt% loading of CNC into the nanocomposite ionogels leads to an appreciable increase of 400% in the Young's modulus. This is due to the interaction of the polymer network with CNC which toughens the ionogels. The unfilled ionogel (100_0 wt% CNC-i-PAACB12-r-PAA) shows stability up to 6% strain while the interlocked ionogel (50_50 wt% CNC-i-PAACB12-r-PAA) remains mechanically stable below 20% strain. This behavior shows typical soft gel behavior. We, therefore, report a great improvement in the mechanical properties of the CNC/LCP nanocomposite ionogels resulting from the dual interlocking. The calculated Young's moduli are shown below.

Youngs modulus for 100_0 wt%

$$\text{CNC-i-PAACB12-r-PAA} = \frac{\text{Rise}}{\text{Run}} = \frac{\Delta\sigma}{\Delta\varepsilon} = \frac{0.002 - 0.0015}{2.75 - 1.75} = 5 \times 10^{-4}\ \text{MPa}$$

Youngs modulus for 50_50 wt%

$$\text{CNC-i-PAACB12-r-PAA} = \frac{\text{Rise}}{\text{Run}} = \frac{\Delta\sigma}{\Delta\varepsilon} = \frac{0.02 - 0.0125}{12.50 - 8.75} = 2 \times 10^{-3}\ \text{MPa}$$

To complement this stress–strain test, we use *S*–*N* curves by dynamic mechanical analysis (DMA) which describe a material's endurance in terms of the number of cycles to failure $N(S)$ when the material is repeatedly cycled at a set stress range. Fig. S14 (ESI†) shows a typical cyclic stress–strain curve obtained with an initial transient behavior where stress required to enforce initial strain decreases leading to cyclic softening and stabilizing after subsequent loading. Initially, these nanocomposite ionogels reached a stress endurance limit of 12.0 MPa which was reduced to 11.4 MPa after 1000 load cycles retaining 95% of the initial stress. Below this limit, we observe a limitless lifetime. Hysteresis curves obtained from 10% strain subjected to 1000 load cycles show a decay of stress over the 1000 cycles for 50_50 wt% CNC-i-PAACB12-r-PAA nanocomposite ionogels. This fatigue test confirms the toughness of these ionogels where compressive stress as a function of the number of points shows no apparent shift in cyclic stress as shown in Fig. S15 (ESI†).

Conclusion

We have designed physical-co-chemical nanocomposite ionogels based on CNC and a smectic LC-containing polyelectrolyte endowed with enhanced rheological behavior and toughness. CNC double networks with different conventional polymers have been widely studied and the LC properties (arising from CNC) reported.[8,26–29] However, double networks involving CNC with different liquid crystalline polymers (LCPs) where there is retention of LC properties (from both CNC and LCP) after interlocking remain unexplored.[8] Our work reports on a CNC double network with a smectic LCP and investigates LC properties resulting from interactions of these two materials. Rheological studies of the interlocked free-standing ionogels demonstrate a typical crosslinked gel behavior with the storage moduli (G') ranging 10^3–10^4 Pa across the entire angular frequency range. Mechanical properties are tailored by varying the concentration of CNCs in the nanocomposite gel. This is attributed to the double network of both chemically crosslinked and physically interlocked networks of the CNC-i-PAACB12-r-PAA. The physical interlocking results from the host–guest interaction between PAACB12-r-PAA and CNC which acts as the rope binding the covalently crosslinked network. Cyclic stress–strain test on 50_50 wt% CNC-i-PAACB12-r-PAA nanocomposite ionogels show that the material retains about 95% of the initial stress after reducing from a stress endurance limit of 12.0 MPa to 11.4 MPa after 1000 load cycles. A dual network wherein the CNC behaves both as a filler and as a network

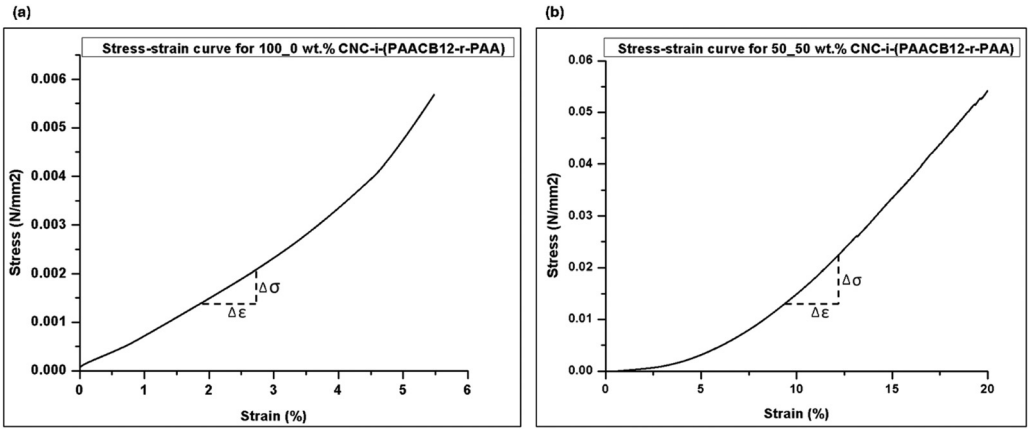

Fig. 9 Effect of CNC concentration on the toughness of nanocomposites. Stress–strain curves for (a) 100_0 wt% CNC-i-PAACB12-r-PAA, and (b) 50_50 wt% CNC-i-PAACB12-r-PAA nanocomposites.

junction improves the tensile properties of the CNC/LCP. This general strategy can be used to develop a double network, mechanically reinforced CNC-based liquid crystalline gels for applications in ion-containing gels,[71–73] actuators,[74,75] and sensors.[76–78]

Data availability

All the data reported in this manuscript are available in tables and figures both in the main manuscript as well as the ESI.†

Conflicts of interest

The authors declare no conflict of interest.

Acknowledgements

This work is supported by the National Science Foundation. SAXS data is partially supported through an NSF grant (MRI-1228817). We also acknowledge funds from Research Excellence Program at the University of Connecticut, Storrs (USA). We acknowledge technical support from the central instrumentation facilities at the Institute of Materials Science and Chemistry Department.

References

1 M. Asem, D. N. Jimat, N. H. S. Jafri, W. M. F. W. Nawawi, N. F. M. Azmin and M. F. Abd Wahab, Entangled cellulose nanofibers produced from sugarcane bagasse via alkaline treatment, mild acid hydrolysis assisted with ultrasonication, *J. King Saud Univ., Eng. Sci.*, 2023, **35**(1), 24–31.
2 S. Elazzouzi-Hafraoui, Y. Nishiyama, J.-L. Putaux, L. Heux, F. Dubreuil and C. Rochas, The shape and size distribution of crystalline nanoparticles prepared by acid hydrolysis of native cellulose, *Biomacromolecules*, 2008, **9**(1), 57–65.
3 L. U. S. Faria, B. J. S. Pacheco, G. C. Oliveira and J. L. Silva, Production of cellulose nanocrystals from pineapple crown fibers through alkaline pretreatment and acid hydrolysis under different conditions, *J. Mater. Res. Technol.*, 2020, **9**(6), 12346–12353.
4 M. El Achaby, N. El Miri, H. Hannache, S. Gmouh and A. Aboulkas, Production of cellulose nanocrystals from vine shoots and their use for the development of nanocomposite materials, *Int. J. Biol. Macromol.*, 2018, **117**, 592–600.
5 A. Tran, C. E. Boott and M. J. MacLachlan, Understanding the Self-Assembly of Cellulose Nanocrystals—Toward Chiral Photonic Materials, *Adv. Mater.*, 2020, **32**(41), 1905876.
6 V. S. Raghuwanshi, C. Browne, W. Batchelor and G. Garnier, Self-assembly of cellulose nanocrystals of different lengths, *J. Colloid Interface Sci.*, 2023, **630**, 249–259.
7 G. Delepierre, S. Eyley, W. Thielemans, C. Weder, E. D. Cranston and J. O. Zoppe, Patience is a virtue: Self-assembly and physico-chemical properties of cellulose nanocrystal allomorphs, *Nanoscale*, 2020, **12**(33), 17480–17493.
8 F. K. Masese, P. K. Njenga, D. M. Ndaya and R. M. Kasi, Recent Advances and Opportunities for Cellulose Nanocrystal-Based Liquid Crystalline Polymer Hybrids and Composite Materials, *Macromolecules*, 2023, **56**(17), 6567–6588.
9 R. A. Chowdhury, S. X. Peng and J. Youngblood, Improved order parameter (alignment) determination in cellulose nanocrystal (CNC) films by a simple optical birefringence method, *Cellulose*, 2017, **24**, 1957–1970.
10 H. Wang, R. Shao, X. Meng, Y. He, Z. Shi, Z. Guo and C. Ye, Programmable Birefringent Patterns from Modulating the Localized Orientation of Cellulose Nanocrystals, *ACS Appl. Mater. Interfaces*, 2022, **14**(31), 36277–36286.
11 S. Peng, Q. Luo, G. Zhou and X. Xu, Recent advances on cellulose nanocrystals and their derivatives, *Polymers*, 2021, **13**(19), 3247.
12 M. S. Reid, M. Villalobos and E. D. Cranston, Cellulose nanocrystal interactions probed by thin film swelling to predict dispersibility, *Nanoscale*, 2016, **8**(24), 12247–12257.

13 T. Aziz, H. Fan, X. Zhang, F. Haq, A. Ullah, R. Ullah, F. U. Khan and M. Iqbal, Advance study of cellulose nanocrystals properties and applications, *J. Polym. Environ.*, 2020, **28**, 1117–1128.
14 J. George, S. Sabapathi and G. Siddaramaiah, Water soluble polymer-based nanocomposites containing cellulose nanocrystals, *Eco-friendly polymer nanocomposites: processing and properties*, 2015, pp. 259–293.
15 D. Trache, M. H. Hussin, M. M. Haafiz and V. K. Thakur, Recent progress in cellulose nanocrystals: sources and production, *Nanoscale*, 2017, **9**(5), 1763–1786.
16 X. Wei, T. Lin, M. Duan, H. Du and X. Yin, Cellulose Nanocrystal-based Liquid Crystal Structures and the Unique Optical Characteristics of Cellulose Nanocrystal Films, *BioResources*, 2021, **16**(1), 2116–2137.
17 K. Ganguly, D. K. Patel, S. D. Dutta, W.-C. Shin and K.-T. Lim, Stimuli-responsive self-assembly of cellulose nanocrystals (CNCs): Structures, functions, and biomedical applications, *Int. J. Biol. Macromol.*, 2020, **155**, 456–469.
18 J. P. Lagerwall, C. Schütz, M. Salajkova, J. Noh, J. Hyun Park, G. Scalia and L. Bergström, Cellulose nanocrystal-based materials: from liquid crystal self-assembly and glass formation to multifunctional thin films, *NPG Asia Mater.*, 2014, **6**(1), e80–e80.
19 B. Risteen, G. Delepierre, M. Srinivasarao, C. Weder, P. Russo, E. Reichmanis and J. Zoppe, Thermally switchable liquid crystals based on cellulose nanocrystals with patchy polymer grafts, *Small*, 2018, **14**(46), 1802060.
20 D. P. Gonçalves and T. Hegmann, Chirality Transfer from an Innately Chiral Nanocrystal Core to a Nematic Liquid Crystal: Surface-Modified Cellulose Nanocrystals, *Angew. Chem., Int. Ed.*, 2021, **60**(32), 17344–17349.
21 L. A. Müller, A. Zingg, A. Arcifa, T. Zimmermann, G. Nyström, I. Burgert and G. Siqueira, Functionalized Cellulose Nanocrystals as Active Reinforcements for Light-Actuated 3D-Printed Structures, *ACS nano*, 2022, **16**(11), 18210–18222.
22 Y. Zheng, Y. Wang, T. Nakajima and J. P. Gong, Effect of predamage on the fracture energy of double-network hydrogels, *ACS Macro Lett.*, 2024, **13**(2), 130–137.
23 H. Bai, Z. Li, S. Zhang, W. Wang and W. Dong, Interpenetrating polymer networks in polyvinyl alcohol/cellulose nanocrystals hydrogels to develop absorbent materials, *Carbohydr. Polym.*, 2018, **200**, 468–476.
24 J. Yang, C.-R. Han, X.-M. Zhang, F. Xu and R.-C. Sun, Cellulose nanocrystals mechanical reinforcement in composite hydrogels with multiple cross-links: correlations between dissipation properties and deformation mechanisms, *Macromolecules*, 2014, **47**(12), 4077–4086.
25 B. R. Estevam, I. D. Perez, Â. M. Moraes and L. V. Fregolente, A review of the strategies used to produce different networks in cellulose-based hydrogels, *Mater. Today Chem.*, 2023, **34**, 101803.
26 M. Tatsumi, Y. Teramoto and Y. Nishio, Polymer composites reinforced by locking-in a liquid-crystalline assembly of cellulose nanocrystallites, *Biomacromolecules*, 2012, **13**(5), 1584–1591.
27 V. Engkagul, C. Rader, N. Pon, S. J. Rowan and C. Weder, Nanocomposites assembled via electrostatic interactions between cellulose nanocrystals and a cationic polymer, *Biomacromolecules*, 2021, **22**(12), 5087–5096.
28 L. G. Germiniani, L. C. da Silva, T. S. Plivelic and M. C. Gonçalves, Poly(ε-caprolactone)/cellulose nanocrystal nanocomposite mechanical reinforcement and morphology: the role of nanocrystal pre-dispersion, *J. Mater. Sci.*, 2019, **54**(1), 414–426.
29 G. Delepierre, H. Traeger, J. Adamcik, E. D. Cranston, C. Weder and J. O. Zoppe, Liquid crystalline properties of symmetric and asymmetric end-grafted cellulose nanocrystals, *Biomacromolecules*, 2021, **22**(8), 3552–3564.
30 J. W. Suen, N. K. Elumalai, S. Debnath, N. M. Mubarak, C. I. Lim and M. M. Reddy, The role of interfaces in ionic liquid-based hybrid materials (ionogels) for sensing and energy applications, *Adv. Mater. Interfaces*, 2022, **9**(34), 2201405.
31 D. Tanaka, T. Mizuno, M. Hara, S. Nagano, I. Saito, K. Yamamoto and T. Seki, Evaluations of mesogen orientation in thin films of polyacrylate with cyanobiphenyl side chain, *Langmuir*, 2016, **32**(15), 3737–3745.
32 J. A. Sirviö, M. Visanko, J. P. Heiskanen and H. Liimatainen, UV-absorbing cellulose nanocrystals as functional reinforcing fillers in polymer nanocomposite films, *J. Mater. Chem. A*, 2016, **4**(17), 6368–6375.
33 J. A. Sirvio, S. Honkaniemi, M. Visanko and H. Liimatainen, Composite films of poly(vinyl alcohol) and bifunctional cross-linking cellulose nanocrystals, *ACS Appl. Mater. Interfaces*, 2015, **7**(35), 19691–19699.
34 P. Liu, X. Guo, F. Nan, Y. Duan and J. Zhang, Modifying Mechanical, Optical Properties and Thermal Processability of Iridescent Cellulose Nanocrystal Films Using Ionic Liquid, *ACS Appl. Mater. Interfaces*, 2017, **9**(3), 3085–3092.
35 J. Qin, Z. Wang, J. Hu, Y. Yuan, P. Liu, L. Cheng, Z. Kong, K. Liu, S. Yan and J. Zhang, Distinct liquid crystal self-assembly behavior of cellulose nanocrystals functionalized with ionic liquids, *Colloids Surf., A*, 2022, **632**, 127790.
36 F. K. Masese, D. Ndaya, C.-H. Liu, N. Eddy, M. D. Morales-Acosta, M.-P. Nieh and R. M. Kasi, Self-assembled materials from cellulose nanocrystals conjugated with a thermotropic liquid crystalline moiety, *Soft Matter*, 2022, **18**(42), 8165–8174.
37 J. A. De La Cruz, Q. Liu, B. Senyuk, A. W. Frazier, K. Peddireddy and I. I. Smalyukh, Cellulose-based reflective liquid crystal films as optical filters and solar gain regulators, *ACS Photonics*, 2018, **5**(6), 2468–2477.
38 S. T. Wu, A semiempirical model for liquid-crystal refractive index dispersions, *J. Appl. Phys.*, 1991, **69**(4), 2080–2087.
39 R. Verma, M. Mishra, R. Dhar and R. Dabrowski, Single walled carbon nanotubes persuaded optimization of the display parameters of a room temperature liquid crystal 4-pentyl-4′ cyanobiphenyl, *J. Mol. Liq.*, 2016, **221**, 190–196.
40 T. D. Ibragimov and R. M. Rzayev, Dielectric relaxation, electric conductivity, and electro-optic properties of SWCNT-doped liquid crystal 5CB, *Fullerenes, Nanotubes Carbon Nanostruct.*, 2020, **28**(12), 982–988.

41 T. Seki, K. Tanaka and K. Ichimura, Photopolymerization of diacetylene Langmuir-Blodgett films on an azobenzene-containing monolayer, *Polym. J.*, 1998, **30**(8), 646–652.
42 M. Jasiurkowska-Delaporte, T. Rozwadowski and E. Juszyńska-Gałązka, Kinetics of non-isothermal and isothermal crystallization in a liquid crystal with highly ordered smectic phase as reflected by differential scanning calorimetry, polarized optical microscopy and broadband dielectric spectroscopy, *Crystals*, 2019, **9**(4), 205.
43 S. J. Cowling, Optical microscopy studies of liquid crystals. *Handbook of Liquid Crystals*, 2014.
44 Y. Geng; J. Noh and J. P. Lagerwall, Transmission polarized optical microscopy of short-pitch cholesteric liquid crystal shells, *Emerging Liquid Crystal Technologies XI*, SPIE, 2016, pp. 71–80.
45 A. Ryabchun and A. Bobrovsky, Cholesteric liquid crystal materials for tunable diffractive optics, *Adv. Opt. Mater.*, 2018, **6**(15), 1800335.
46 J. Yang, C.-R. Han, J.-F. Duan, F. Xu and R.-C. Sun, Mechanical and viscoelastic properties of cellulose nanocrystals reinforced poly(ethylene glycol) nanocomposite hydrogels, *ACS Appl. Mater. Interfaces*, 2013, **5**(8), 3199–3207.
47 J. Yang, C.-R. Han, J.-F. Duan, M.-G. Ma, X.-M. Zhang, F. Xu, R.-C. Sun and X.-M. Xie, Studies on the properties and formation mechanism of flexible nanocomposite hydrogels from cellulose nanocrystals and poly(acrylic acid), *J. Mater. Chem.*, 2012, **22**(42), 22467–22480.
48 T. Zhang, T. Zuo, D. Hu and C. Chang, Dual physically cross-linked nanocomposite hydrogels reinforced by tunicate cellulose nanocrystals with high toughness and good self-recoverability, *ACS Appl. Mater. Interfaces*, 2017, **9**(28), 24230–24237.
49 J. Yang and C. Han, Mechanically viscoelastic properties of cellulose nanocrystals skeleton reinforced hierarchical composite hydrogels, *ACS Appl. Mater. Interfaces*, 2016, **8**(38), 25621–25630.
50 R. S. Shah, S. Bryant and M. Trifkovic, Microstructural rearrangements and their rheological signature in coarsening of cocontinuous polymer blends, *Macromolecules*, 2020, **53**(24), 10918–10926.
51 A.-C. Genix and J. Oberdisse, Structure and dynamics of polymer nanocomposites studied by X-ray and neutron scattering techniques, *Curr. Opin. Colloid Interface Sci.*, 2015, **20**(4), 293–303.
52 J. Yang, L.-H. Deng, C.-R. Han, J.-F. Duan, M.-G. Ma, X.-M. Zhang, F. Xu and R.-C. Sun, Synthetic and viscoelastic behaviors of silica nanoparticle reinforced poly(acrylamide) core–shell nanocomposite hydrogels, *Soft Matter*, 2013, **9**(4), 1220–1230.
53 H. Li, M. Kruteva, K. Mystek, M. Dulle, W. Ji, T. R. Pettersson and L. Wågberg, Macro-and microstructural evolution during drying of regenerated cellulose beads, *ACS Nano*, 2020, **14**(6), 6774–6784.
54 J. G. Nam, K. H. Ahn, S. J. Lee and K. Hyun, Strain stiffening of non-colloidal hard sphere suspensions dispersed in Newtonian fluid near liquid-and-crystal coexistence region, *Rheol. Acta*, 2011, **50**, 925–936.
55 O. S. Nnyigide, A Study of Bovine Serum Albumin (BSA) Hydrogel with Various Chemical Denaturants by Rheological Measurements and Molecular Dynamics Simulation, *PhD Thesis*, Pusan National University, 2019.
56 O. S. Nnyigide and K. Hyun, Effects of anionic and cationic surfactants on the rheological properties and kinetics of bovine serum albumin hydrogel, *Rheol. Acta*, 2018, **57**, 563–573.
57 A. A. Moud and A. A. Moud, Flow and assembly of cellulose nanocrystals (CNC): A bottom-up perspective-A review, *Int. J. Biol. Macromol.*, 2023, 123391.
58 A. A. Moud, M. Kamkar, A. Sanati-Nezhad, S. H. Hejazi and U. Sundararaj, Viscoelastic properties of poly(vinyl alcohol) hydrogels with cellulose nanocrystals fabricated through sodium chloride addition: Rheological evidence of double network formation, *Colloids Surf., A*, 2021, **609**, 125577.
59 C. Tom, S. N. Sangitra and R. K. Pujala, Rheological fingerprinting and applications of cellulose nanocrystal based composites: A review, *J. Mol. Liq.*, 2023, **370**, 121011.
60 C. Gauche and M. I. Felisberti, Colloidal behavior of cellulose nanocrystals grafted with poly(2-alkyl-2-oxazoline) s, *ACS Omega*, 2019, **4**(7), 11893–11905.
61 S. Shafiei Sabet, *Shear rheology of cellulose nanocrystal (CNC) aqueous suspensions*, University of British Columbia, 2013, DOI: **10.14288/1.0165728**.
62 A. Rao, T. Divoux, G. H. McKinley and A. J. Hart, Shear melting and recovery of crosslinkable cellulose nanocrystal–polymer gels, *Soft Matter*, 2019, **15**(21), 4401–4412.
63 V. Calabrese, S. Varchanis, S. J. Haward, J. Tsamopoulos and A. Q. Shen, Structure-property relationship of a soft colloidal glass in simple and mixed flows, *J. Colloid Interface Sci.*, 2021, **601**, 454–466.
64 J. De la Fuente, M. Wilhelm, H. W. Spiess, E. Madruga, M. Fernandez-Garcia and M. Cerrada, Thermal, morphological and rheological characterization of poly(acrylic acid-g-styrene) amphiphilic graft copolymers, *Polymer*, 2005, **46**(13), 4544–4553.
65 R. Pettau, T. Müller, M. Khazimullin, I. Rehberg and H.-W. Schmidt, Structure-property relations of liquid crystalline gels with ABA-triblock copolymers as gelators, *Z. Phys. Chem.*, 2012, **226**(7–8), 645–664.
66 O. O. Mykhaylyk, N. J. Warren, A. J. Parnell, G. Pfeifer and J. Laeuger, Applications of shear-induced polarized light imaging (SIPLI) technique for mechano-optical rheology of polymers and soft matter materials, *J. Polym. Sci., Part B: Polym. Phys.*, 2016, **54**(21), 2151–2170.
67 S. Azizi, M. B. Ahmad, M. Z. Hussein, N. A. Ibrahim and F. Namvar, Preparation and properties of poly(vinyl alcohol)/chitosan blend bionanocomposites reinforced with cellulose nanocrystals/ZnO–Ag multifunctional nanosized filler, *Int. J. Nanomed.*, 2014, **9**, 1909.
68 M. B. Agustin, B. Ahmmad, E. R. P. De Leon, J. L. Buenaobra, J. R. Salazar and F. Hirose, Starch-based biocomposite films reinforced with cellulose nanocrystals from garlic stalks, *Polym. Compos.*, 2013, **34**(8), 1325–1332.
69 M. Younas, A. Noreen, A. Sharif, A. Majeed, A. Hassan, S. Tabasum, A. Mohammadi and K. M. Zia, A review on

versatile applications of blends and composites of CNC with natural and synthetic polymers with mathematical modeling, *Int. J. Biol. Macromol.*, 2019, **124**, 591–626.

70 P. S. Nagendra, V. Prasad and K. Ramji, A study on dynamic mechanical analysis of natural nano banana particle filled polymer matrix composites, *Mater. Today: Proc.*, 2017, **4**(8), 9081–9086.

71 A. R. Khokhlov and E. Dormidontova, Self-organization in ion-containing polymer systems, *Phys.-Usp.*, 1997, **40**(2), 109.

72 Y. Song, T. Gotoh and S. Nakai, Simultaneous Removal of Anionic and Cationic Species by Ionic Hydrogels via Positively Charged Complex: Adsorption Mechanism of Arsenic(v) and Chromium(iii) in Highly Acidic System, *ACS ES&T Water*, 2024, **4**(5), 2005–2017.

73 C. Chen, B. Mei, J. Zhou, K. S. Schweizer, C. M. Evans and P. V. Braun, Coupling of Ethylene-Oxide-Based Polymeric Network Structure and Counterion Chemistry to Ionic Conductivity and Ion Selectivity, *Macromolecules*, 2024, **57**(14), 6779–6788.

74 W. Sun, Z. Song, J. Wang, Z. Yi and M. He, Preparation of patterned hydrogels for anti-counterfeiting and directional actuation by shear-induced orientation of cellulose nanocrystals, *Carbohydr. Polym.*, 2024, **332**, 121946.

75 M. He, Y.-I. Hsu and H. Uyama, High-performance bioinspired multi-responsive chiral cellulose nanocrystals-based flexible films for information encryption, *Chem. Eng. J.*, 2024, **495**, 153516.

76 S. Singh, S. Bhardwaj, P. Tiwari, K. Dev, K. Ghosh and P. K. Maji, Recent advances in cellulose nanocrystals-based sensors: a review, *Mater. Adv.*, 2024, **5**, 2622–2654.

77 Y. Wang, A. Yao, B. Dou, C. Huang, L. Yang, J. Liang, J. Lan and S. Lin, Self-healing, environmentally stable and adhesive hydrogel sensor with conductive cellulose nanocrystals for motion monitoring and character recognition, *Carbohydr. Polym.*, 2024, **332**, 121932.

78 P. Rahmani, A. Shojaei and M. D. Dickey, A highly conductive and ultra-stretchable polyaniline/cellulose nanocrystal/polyacrylamide hydrogel with hydrophobic associations for wearable strain sensors, *J. Mater. Chem. A*, 2024, **12**(16), 9552–9562.